JOURNAL OF MATERIALS SCIENCE 37 (2002) 2651 – 2658

Modal separation of work-of-fracture of carbon/carbon composites

K. YASUDA*, S. TANAKA, Y. MATSUO
Department of Metallurgy and Ceramics Science,
Graduate School of Science and Engineering, Tokyo Institute of Technology,
2-12-1 Ookayama, Meguro-ku, Tokyo 152-8552, Japan
E-mail: kyasuda@ceram.titech.ac.jp

Modal separation of work-of-fracture was carried out for unidirectional C/C composites in order to characterize their multi-modal fracture behavior. The C/C composites were prepared by filament winding method with a coal tar pitch as a matrix precursor, and followed by heat treatment at temperatures between 1000°C and 2800°C under argon flow. During single edge-notched beam tests, tensile fracture and interlaminar shear fracture were simultaneously observed in the specimens. In proportion to the fracture surface area, the total work done during fracture was divided into each fracture mode, and the modal work-of-fracture was obtained by dividing each modal dissipation energy by twice the corresponding modal fracture surface area. With increasing the heat treatment temperature, the modal work-of-fracture for the tensile mode gradually increased and reached a maximum of around 6 kJm^{-2} at a heat treatment temperature of 2000°C, whereas the modal work-of-fracture for the interlaminar shear mode remained constant around 20 Jm^{-2}. Determination of these modal work-of-fracture values revealed quantitatively the contribution of each fracture mode to the total dissipation energy of the composites.

1. Introduction

Carbon/Carbon composites (C/C composites) have been considered promising materials for structural applications at high temperatures. Currently, a few types of C/C composites are used in the aerospace industry because of their useful characteristics including lightweight, high stiffness, no degradation in strength at high temperatures, high fracture resistance, and high thermal shock resistance. However, there remain some problems to be solved regarding C/C composite technology: high fabrication cost, low oxidation resistance, insufficient understanding of materials design, and poor reliability control of component design.

In the last three decades, much effort has been made to develop processing technology for C/C composites [1]; however, some researchers have taken interest in the fracture mechanics of C/C composites in order to collect fundamental information on reliability control. Guess and Hoover [2] conducted single edge-notched beam tests on two different C/C composites. They concluded that the critical stress intensity factor (K_{IC}) was not considered as a material constant if macroscopic interlaminar shear fracture occurred, and that the work-of-fracture (γ_{WOF}) was also dependent on the experimental conditions. Hettche and Tucker [3] determined the K_{IC} values of the same C/C composites, and recognized the strong influence of interlaminar shear fracture on the values in their experiments as well. Zhao *et al*. [4] reported the changes in γ_{WOF} affected by fiber architecture. In 1985, Kim *et al*. [5] showed the influence of edge and flatwise specimen geometries on the K_{IC} and the K_R-curve of a C/C composite. The edgewise specimens were fractured in a tensile mode along an initial crack; however, the flatwise specimens were fractured in an interlaminar shear mode perpendicular to the initial crack. This indicated that estimation of the K_{IC} and the K_R-curve was valid for the edgewise specimens but not for the flatwise specimens. Therefore, Kim *et al*. suggested that adequate parameters are needed in order to separately consider each fracture mode in such highly anisotropic materials. This is the first point to be discussed in this paper.

After Kim's paper, the main theme in this field moved to K_R-curve estimation. Jenkins *et al*. [6], Senet *et al*. [7], Sakai *et al*. [8], and Griesheim *et al*. [9] reported the K_R-curves of C/C composites independently. Similar to Kim's result, Jenkins *et al*. also obtained a nonlinear rising K_R-curve of a C/C composite. Sakai *et al*. emphasized that the rising K_R-curve of C/C composites was induced by fiber bridging and pullout mechanisms, and also suggested that "essential work-of-fracture" should be used for the materials having the rising K_R-curve effect in place of the work-of-fracture. This "essential work-of-fracture" was originally proposed by Mai and

*Author to whom all correspondence should be addressed.

Pilko [10] taking the nonlinear contribution of a large-scale frontal process zone into consideration. Based on their researches, we currently tend to consider that K_{IC} and γ_{WOF} values must be affected by the rising K_R-curve effect, which depends on the specimen size and geometry as well as testing conditions. However, such a conclusion can be adopted after we check how much the coexisting fracture modes (e.g., interlaminar shear fracture in Guess and Hoover's paper) influence these values. Or rather, by focusing on multi-modal fracture behavior itself, we should know how much each fracture mode contributes to the total dissipation energy in a composite material. This is the second point to be discussed in this paper.

The purpose of this paper is to conduct modal separation of the work-of-fracture of C/C composites, and to show the contribution of each fracture mode to the total dissipation energy during fracture. First, we introduce the "modal work-of-fracture" concept which was previously proposed by the authors as the "modal fracture energy" [11]. Secondly, we show the experimental results of single edge-notched beam tests of C/C composites heat-treated at different temperatures and how to obtain the modal work-of-fracture for tensile and interlaminar shear modes. Finally, in order to characterize the multi-modal fracture behavior of the C/C composites, we discuss how the modal work-of-fracture values change depending on the heat treatment temperature.

2. Concept of modal separation of work-of-fracture

Consider that several macroscopic fracture modes simultaneously appear during a work-of-fracture test of a composite material. Based on the energy conservation law, the total dissipation energy during fracture, U_{total}, can be obtained as the sum of each modal dissipation energy U_i as follows,

$$U_{total} = \sum_{i=1}^{n} U_i, \tag{1}$$

where n is the total number of fracture modes. Up to now, we have mainly used the work-of-fracture γ_{WOF} for such a composite material. The definition of γ_{WOF} is as follows,

$$\gamma_{WOF} = \frac{U_{total}}{2S_{tensile}} = \frac{U_{tensile} + U_{shear} + \cdots}{2S_{tensile}}, \tag{2}$$

where $U_{tensile}$ is the modal dissipation energy for the tensile mode, and $S_{tensile}$ is the modal fracture surface area for the tensile mode (viz. the nominal area of the notch ligament). However, we see that γ_{WOF} does not have clear physical meaning because the numerator in Equation 2 contains not only $U_{tensile}$ but also other modal dissipation energies such as $U_{shear,}$ etc. Therefore, by dividing each modal dissipation energy U_i by twice the corresponding modal fracture surface area $2S_i$, we newly define the "modal work-of-fracture" γ_i by the following equation,

$$\gamma_i = \frac{U_i}{2S_i}, \tag{3}$$

where γ_i is assumed to be a material constant. If we estimate all the modal work-of-fracture values of the composite material, we can discuss the fracture resistance by drawing a clear distinction between the fracture modes.

In order to estimate the modal work-of-fracture γ_i, we rewrite Equation 1 with γ_i as,

$$U_{total} = \sum_{i=1}^{n} 2\gamma_i S_i. \tag{4}$$

The total fracture surface area S_{total} is also defined as,

$$S_{total} = \sum_{i=1}^{n} S_i. \tag{5}$$

By dividing Equation 4 by $2S_{total}$, we obtain the following equation,

$$\frac{U_{total}}{2S_{total}} = \sum_{i=1}^{n} \gamma_i \frac{S_i}{S_{total}} = \sum_{i=1}^{n-1} (\gamma_i - \gamma_n) \frac{S_i}{S_{total}} + \gamma_n. \quad \left(\because \sum_{i=1}^{n} \frac{S_i}{S_{total}} = 1 \right) \tag{6}$$

This equation represents a hyperplane in a $(n+1)$-dimensional space with bases of $U_{total}/2S_{total}$ and S_i/S_{total} ($i = 1 \sim n$). In order to obtain each value of γ_i, we extrapolate the value of $U_{total}/2S_{total}$ when the corresponding S_i/S_{total} approaches 1. Equation 6 is a fundamental equation for modal separation of work-of-fracture.

We have known that each modal dissipation energy U_i also consists of several dissipation energies in a microscopic scale: the surface energy (for creating new surfaces), the frontal process zone energy (for stress relaxation mechanisms in the frontal process zone by dislocation or microcrack), the crack-face interaction energy (for contact and zone shielding mechanisms in the process zone wake), and other unknown dissipation energies (for example, emitting sound during fracture). The contribution of each microscopic dissipation process to the modal dissipation energy will change with crack extension if a material has a rising K_R-curve effect. However, the contributions of each of these processes can not be perfectly distinguished; thus, in this study we shall limit ourselves to a discussion of modal separation on a macroscopic scale and focus on the multi-modal fracture behavior of composite materials.

3. Experimental

3.1. Specimen preparation

A coal tar pitch was used as a matrix precursor, and its characteristics are summarized in Table I. Unidirectional preforms were made by filament winding method using a PAN-based carbon fiber (TORAYCA, T300B-3000-40B, 3000 filaments) and a solution of the pitch in benzene. After being dried over a hotplate, the preforms were hot-pressed at 500°C for 1 hour under a pressure of 2.3 kPa, and carbonized at 1000°C for 1 hour under argon flow. Finally, the carbonized composites were

TABLE I Characteristics of the coal tar pitch

Softening point (°C)	85
Fixed carbon (%)	54
Toluene insoluble (%)	13
Quinoline insoluble (%)	Trace
Specific gravity	1.26
Average molecular weight	400

heat-treated for 1 hour under argon flow at 1200°C, 1500°C, 2000°C, 2500°C, and 2800°C, respectively.

3.2. Characterization

The bulk density was calculated from the mass and dimensions of the specimen. The apparent density was measured by Archimedes method. The true density was determined by pycnometry with benzene as an immersion medium. The total porosity was calculated from the true density and the bulk density, and was regarded as the volume fraction of the pores. The volume fractions of the matrix and the fibers were estimated by image analysis using optical micrographs. X-ray diffraction analysis was also carried out using Ni-filtered Cu K_α radiation. The (002) XRD profile was separated into matrix and fiber components by curve fitting analysis, and the interlayer spacing and the crystallite size were estimated according to the JSPS method [12]. Three point-bending tests were carried out on smooth specimens (4 mm in breadth × 1.5 mm in width × 40 mm in length) under a crosshead speed of 0.1 mm/min. The span was 30 mm. The Young's modulus and the bending strength were obtained from the load/displacement curves.

In order to characterize the fiber/matrix interface of the composites, fiber push-in tests were carried out using a micro compression testing machine (Shimazu: MCTM-500). A small specimen was molded using an epoxy resin, and a pair of surfaces normal to the fiber orientation was obtained by polishing. Berkovich indentation was conducted at a center of a fiber appeared on the polished surface under a loading rate of 0.53 mN/s, and a load/displacement curve was then recorded. The thickness of the specimen was 1 mm. The applied load was changed from 40 mN to 100 mN depending on the heat treatment temperature of the specimens. The sliding force at the fiber/matrix interface was determined based on the onset load of a large displacement shift in the load/displacement curve.

3.3. Work-of-fracture test

As shown in Fig. 1, three types of specimen dimensions (A, B, C) were prepared for each C/C composite in order to alter each contribution of the modal dissipation energy to the total dissipation energy. The fiber orientation was adjusted to the longitudinal direction of the specimen. A straight-through notch was introduced into the specimen perpendicular to the fiber orientation. For the same purpose as these relating to the specimen dimensions, the relative notch length a_0/W was also changed from 1/4 to 3/4 for each type of specimen dimensions, where a_0 is the notch length, and W is the width of the specimen. The notch tip was finished with

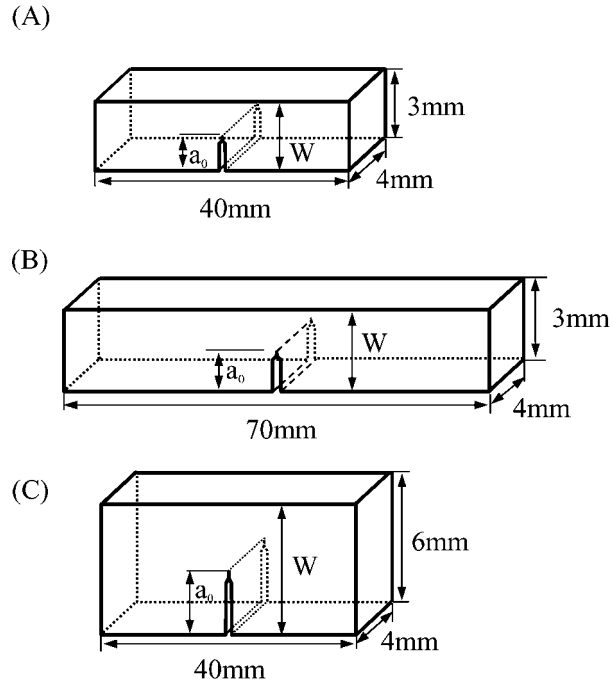

Figure 1 Three types of specimen dimensions for work-of-fracture tests.

a sharp razor blade in order to reduce the notch radius to less than 10 μm. The three-point bending tests were carried out under a cross-head speed of 0.5 mm/min until the notched specimens were fractured completely. The span was 30 mm for type A and B specimens, and 60 mm for type C specimens.

3.4. Modal separation of work-of-fracture

As discussed later, we found that two fracture modes (tensile fracture and interlaminar shear fracture) simultaneously appeared in the specimens during the work-of-fracture tests. Therefore, Equation 6 can be rewritten into the following,

$$\frac{U_{\text{total}}}{2S_{\text{total}}} = \gamma_{\text{tensile}}\frac{S_{\text{tensile}}}{S_{\text{total}}} + \gamma_{\text{shear}}\frac{S_{\text{shear}}}{S_{\text{total}}}$$
$$= (\gamma_{\text{tensile}} - \gamma_{\text{shear}})\frac{S_{\text{tensile}}}{S_{\text{total}}} + \gamma_{\text{shear}}. \quad (7)$$
$$\left(\because \frac{S_{\text{tensile}}}{S_{\text{total}}} + \frac{S_{\text{Shear}}}{S_{\text{total}}} = 1\right)$$

This equation shows that $U_{\text{total}}/2S_{\text{total}}$ is a linear function of $S_{\text{tensile}}/S_{\text{total}}$ with a slope of $(\gamma_{\text{tensile}} - \gamma_{\text{shear}})$ and a y-intercept of γ_{shear}. Therefore, γ_{tensile} can be obtained from the extrapolated value of $U_{\text{total}}/2S_{\text{total}}$ when $S_{\text{tensile}}/S_{\text{total}}$ approaches 1, and also γ_{shear} can be obtained from the extrapolated value of $U_{\text{total}}/2S_{\text{total}}$ when $S_{\text{tensile}}/S_{\text{total}}$ approaches 0. Here, the total dissipation energy U_{total} was calculated from an area under a load/displacement curve, the tensile fracture surface area S_{tensile} was given by the product of the length of the notch ligament and the breadth of the specimen, and the interlaminar shear fracture surface area S_{shear} was given by the product of the total length of macroscopic interlaminar shear cracks and the breadth of the specimen. In particular, the length of a macroscopic

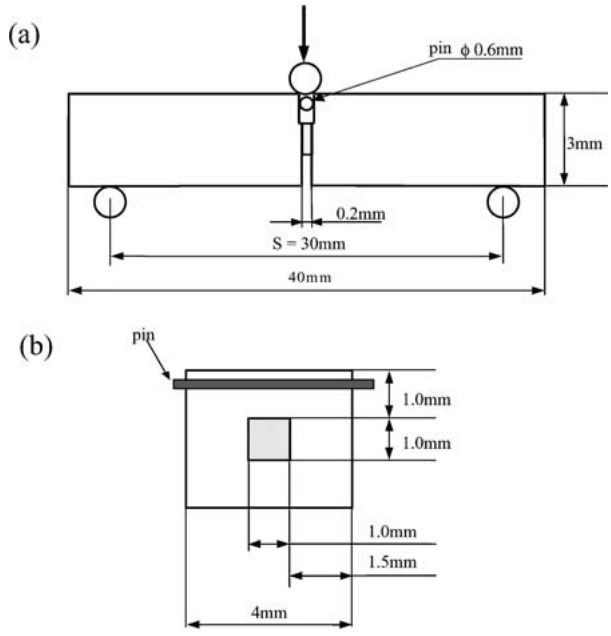

Figure 2 Fiber pullout energy measurement; (a) three-point bending specimen geometry with a circumferential notch, (b) the cross section at the notch.

interlaminar shear crack was carefully measured by stereomicroscopy throughout the specimen in both side views.

Additionally, we calculated the work-of-fracture γ_{WOF} for comparative study. From the definition of γ_{WOF}, we have already known that γ_{WOF} can be applied if and only if a specimen is fractured in a tensile mode. Further, we tried to estimate the essential work-of-fracture by plotting γ_{WOF} against the ligament length and by extrapolating its value when the ligament length approached zero [10].

3.5. Verification of the modal work-of-fracture for the tensile mode $\gamma_{tensile}$

We briefly checked the modal work-of-fracture for the tensile mode $\gamma_{tensile}$. As shown in Fig. 2, a deep circumferential notch was introduced into a JIS-type specimen according to the method of Miyajima and Sakai [13]. The nominal area of the notch ligament was determined in order to leave almost the same order of the fiber pullout length as that in the case of the work-of-fracture tests. A small steel pin (ϕ0.6 mm) was inserted in the slit of the rear notch, and the three-point bending tests were carried out under a crosshead speed of 0.5 mm/min until the specimens were fractured completely. The fiber pullout energy $\gamma_{pullout}$ was calculated by dividing the total dissipation energy by twice the nominal area of the notch ligament, and was compared with the modal work-of-fracture for the tensile mode $\gamma_{tensile}$.

4. Results and discussion

4.1. Characterization of specimens

Table II summarizes the characterization of the C/C composites addressed in this study. The texture of the matrix carbon was classified as the coarse flow-type in each C/C composite. Note that the volume fractions of carbon fibers, the matrix carbon, and pores are almost

TABLE II Characterization of the C/C composites

	HTT[a](°C)					
	1000	1200	1500	2000	2500	2800
Texture	Flow	Flow	Flow	Flow	Flow	Flow
Bulk density (gcm^{-3})	1.38	1.40	1.39	1.42	1.47	1.51
Apparent density (gcm^{-3})	1.58	1.59	1.60	1.66	1.75	1.75
True density (gcm^{-3})	1.78	1.81	1.81	1.82	1.90	1.91
Fiber volume fraction (%)	50	49	51	53	54	54
Matrix volume fraction (%)	28	29	26	25	23	24
Porosity (%)	22	22	23	22	23	21
Young's modulus (GPa)	109	121	103	88	105	124
Bending strength (MPa)	174	181	180	163	183	155

[a] Heat treatment temperature.

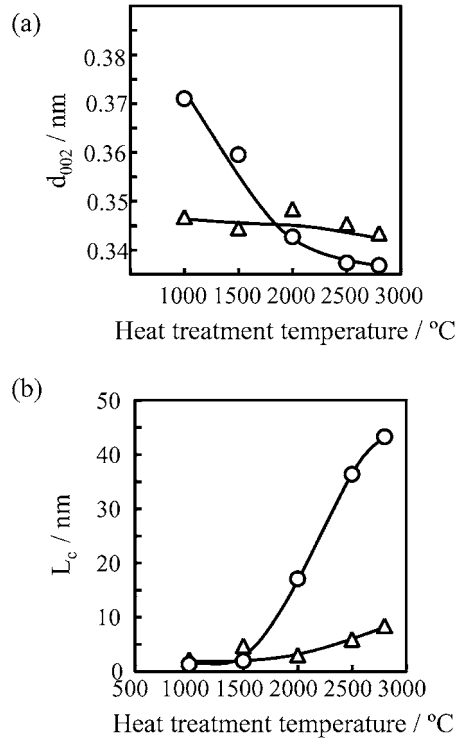

Figure 3 Interlayer spacing d_{002} and crystallite size L_c of the matrix carbon (○) and carbon fibers (△).

constant around 52%, 26%, and 22%, respectively. The Young's modulus and the bending strength also do not largely change with increasing the heat treatment temperature. Fig. 3 reveals that the matrix carbon begins to graphitize at around a heat treatment temperature of 1500°C and is almost complete at around 2500°C.

4.2. Work-of-fracture test

All the specimens were stably fractured during the work-of-fracture tests, and valid load/displacement curves were obtained. The typical appearances of the specimens after the tests are shown in Fig. 4. Only the tensile fracture can be seen in the specimen heat-treated at 1000°C, whereas both tensile fracture and

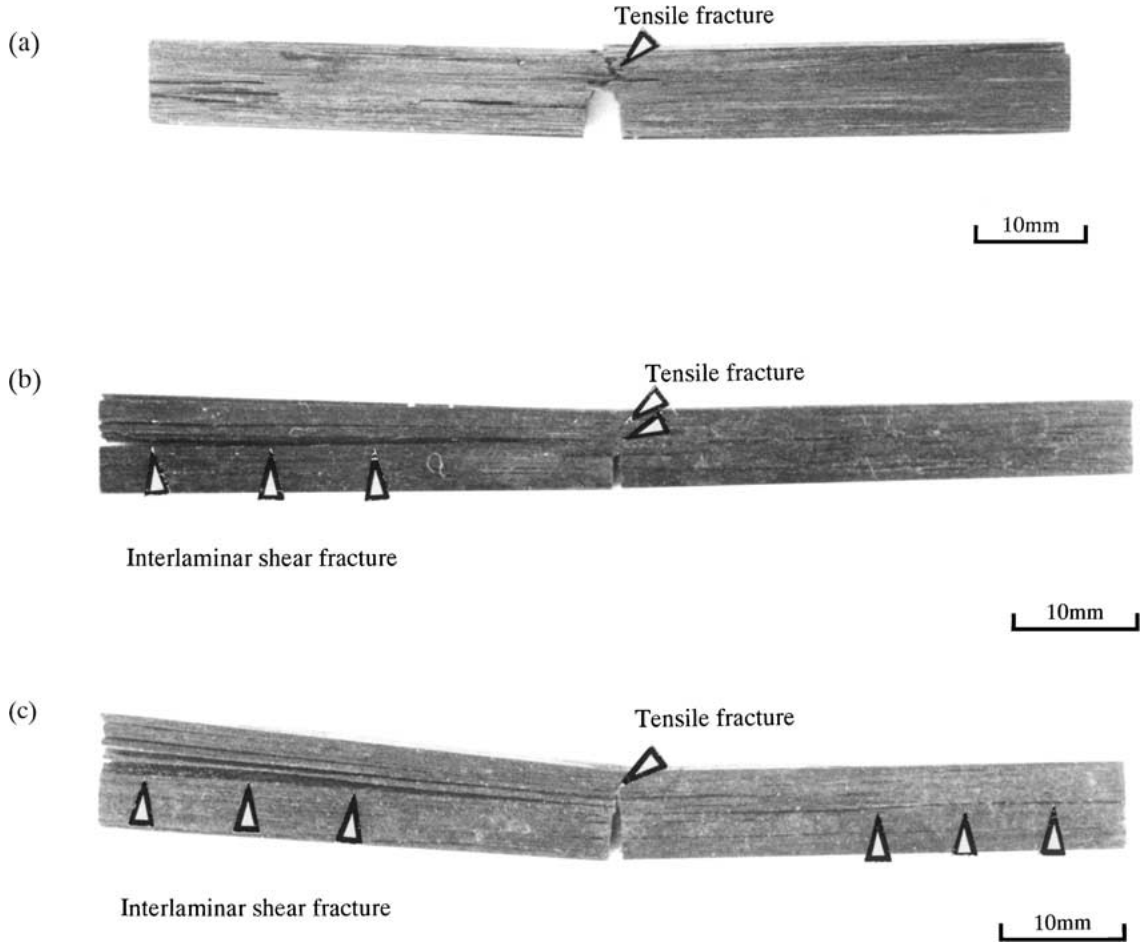

Figure 4 Appearances of specimens after work-of-fracture tests; (a) HTT1000°C, (b) HTT2000°C, (c) HTT2500°C.

interlaminar shear fracture can be seen in the specimens heat-treated at 2000°C and 2500°C. There was a tendency for interlaminar shear fracture to increase with the heat treatment temperature. Thus, we obtained suitable specimens to investigate the modal separation of work-of-fracture.

Prior to modal separation, we shall review the work-of-fracture γ_{WOF} and the essential work-of-fracture. Fig. 5 shows the relation between the calculated γ_{WOF} and ligament length. Open circles, open triangles and open squares denote datapoints of type A, B, and C specimens, respectively. For the specimen heat-treated at 1000°C, γ_{WOF} does not depend on the type of specimen, and produces a monotonously increasing curve with the ligament length. So, we extrapolate the γ_{WOF} value along this curve when the ligament length approaches zero, and obtain 0.62 kJm^{-2} as the essential work-of-fracture of the specimen heat-treated at 1000°C. On the other hand, we do not find any explicit tendency in γ_{WOF} for the specimens heat-treated at 2000°C and 2500°C, and realize that γ_{WOF} and the essential work-of-fracture are not always useful for composite materials. As pointed out in Chapter 2, γ_{WOF} can be applied if and only if a specimen is fractured in a tensile mode (viz. single modal fracture). And also the essential work-of-fracture is just modified by taking the rising K_R-curve effect into consideration. However, the specimens heat-treated at higher temperatures actually show the multi-modal fracture with tensile and

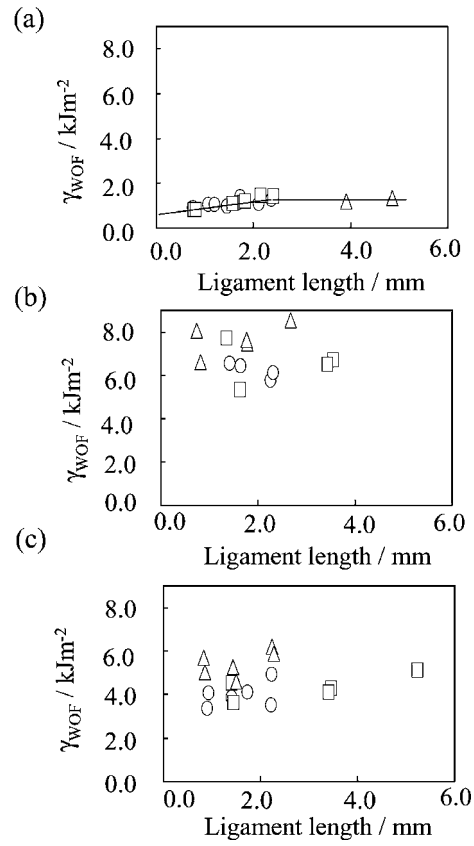

Figure 5 Relation between γ_{WOF} and ligament length, (a) HTT1000°C, (b) HTT2000°C, (c) HTT2500°C, ○: type A, △: type B, □: type C.

interlaminar shear modes. Therefore, we see large data scattering in Fig. 5b and c, and fully understand that the most significant issue regarding composite materials is how to deal with multi-modal fracture behavior rather than K_R-curve effects.

4.3. Modal separation of work-of-fracture

According to Equation 7, we plot $U_{total}/2S_{total}$ against $S_{tensile}/S_{total}$ for each C/C composite. Fig. 6 shows the plots for the specimens heat-treated at 1000°C, 2000°C, and 2500°C, respectively. Although the relative notch length and the specimen dimensions are quite different, we find that datapoints are almost on a straight line for each C/C composite. Their correlation coefficients (r) are estimated to be 0.91–0.99. From these figures, we understand that modal separation of work-of-fracture has been performed satisfactorily, and also that no concern with the rising K_R-curve effect has not caused any fatal error in the modal separation as seen in the linearity in Fig. 6.

By regression analysis, we obtain the modal work-of-fracture for the tensile mode $\gamma_{tensile}$ ($S_{tensile}/S_{total} = 1$) and for the interlaminar shear mode γ_{shear} ($S_{tensile}/S_{total} = 0$). These values are plotted as open circles in Fig. 7. The error bar denotes the standard deviation of the estimated value. For the tensile mode, $\gamma_{tensile}$ is around 1.0 kJm^{-2} for the specimen heat-treated at 1000°C. With increasing the heat treatment temperature, $\gamma_{tensile}$ gradually increases and reaches a maximum around 6.0 kJm^{-2} at a heat treatment temperature of 2000°C. Then, $\gamma_{tensile}$ decreases at heat treatment temperatures above 2000°C. On the other hand, for the interlaminar shear mode, γ_{shear} remains constant around 20 Jm^{-2}, independent of the heat treatment temperature.

We consider that γ_{shear} is accurately estimated because most of the datapoints are near its extrapolated point in Fig. 6. However, we do not have sufficient datapoints near the extrapolated point of $\gamma_{tensile}$, especially in the specimens heat-treated at higher temperatures. Thus, we tried to measure the fiber pullout energy $\gamma_{pullout}$ in order to verify $\gamma_{tensile}$ using a different method. The closed circles in Fig. 7a denote $\gamma_{pullout}$, and we find that $\gamma_{tensile}$ coincides well with $\gamma_{pullout}$ at any heat treatment temperature. Since Miyajima and Sakai [13] reported that the greater part of $\gamma_{tensile}$ was occupied by $\gamma_{pullout}$ in some C/C composites, this coincidence indicates that $\gamma_{tensile}$ is also well estimated even if the datapoints are distributed far from the extrapolated point.

4.4. Dependence of $\gamma_{tensile}$ and γ_{shear} on heat treatment temperature

Fig. 8a and b show both changes in the sliding force at the fiber/matrix interface and also the fiber pullout length in the work-of-fracture test specimens. With increasing the heat treatment temperature, the sliding force monotonously decreases, whereas the fiber pullout length slightly increases and reaches a maximum at a heat treatment temperature between 2000°C and 2500°C. If we recognize that their product correlates positively with the dissipation energy induced by fiber pullout, we can understand phenomenologically that $\gamma_{tensile}$ has a maximum at around a heat treatment temperature of 2000°C.

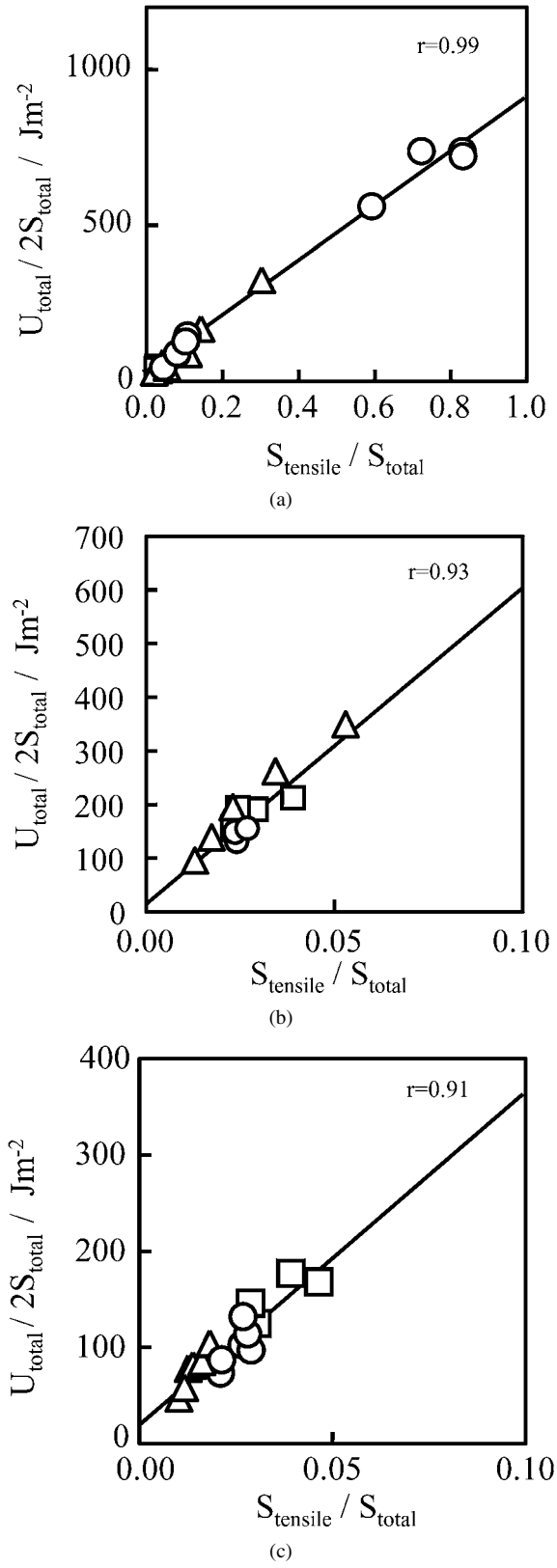

Figure 6 (a) Relation between $U_{total}/2S_{total}$ and $S_{tensile}/S_{total}$ of the specimen (HTT1000°C), ○: type A, △: type B, □: type C. (b) Relation between $U_{total}/2S_{total}$ and $S_{tensile}/S_{total}$ of the specimen (HTT2000°C), ○: type A, △: type B, □: type C. (c) Relation between $U_{total}/2S_{total}$ and $S_{tensile}/S_{total}$ of the specimen (HTT2500°C), ○: type A, △: type B, □: type C.

No adequate explanation exists regarding the change in γ_{shear}. We just suggest the correlation between γ_{shear}

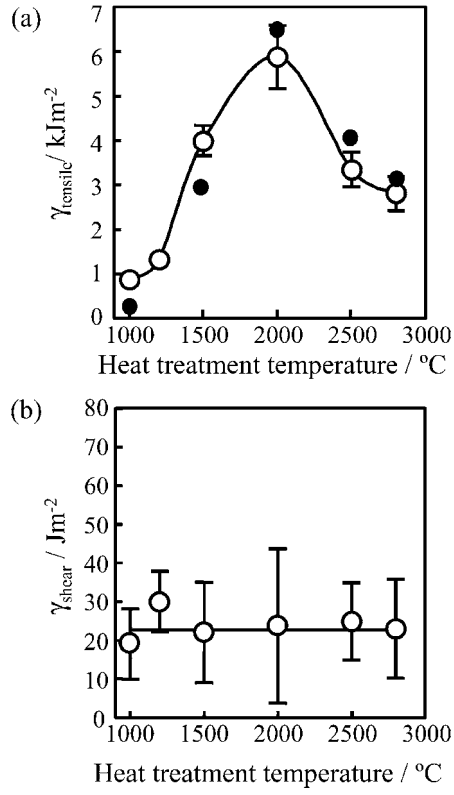

Figure 7 Dependence of modal work-of-fracture on HTT, ○: $\gamma_{tensile}$ and γ_{shear}, ●: $\gamma_{pullout}$.

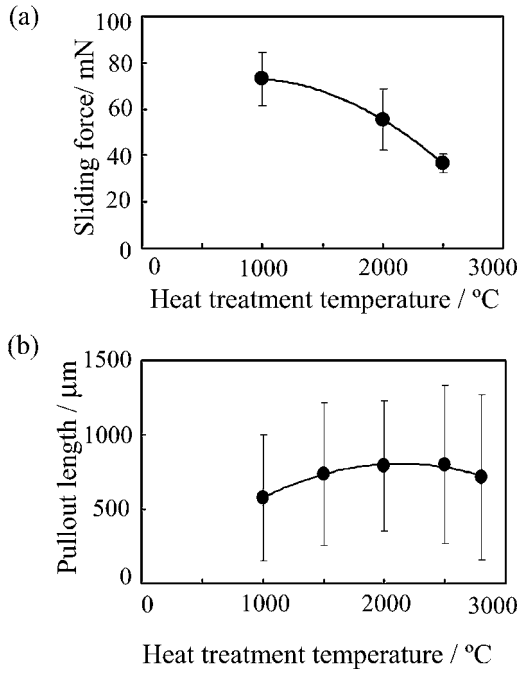

Figure 8 Changes in sliding force at the interface and pullout length of fiber.

and the debris density on interlaminar shear fracture surfaces from a preliminary experiment. The relation will be discussed in the future.

4.5. Contribution of each fracture mode to total energy dissipation

Finally, we reconstruct the total dissipation energy U_{total} by using the estimated modal work-of-fracture

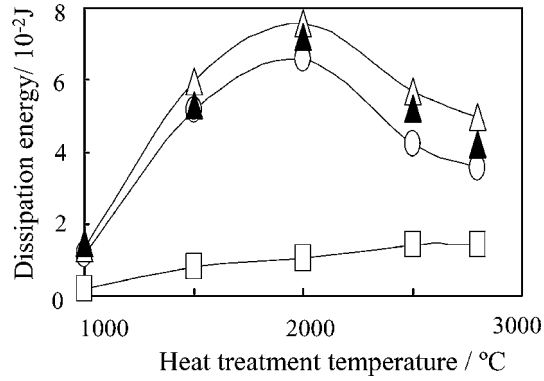

Figure 9 Changes in dissipation energies with HTT, ○: $U_{tensile}$, □: U_{shear}, △: U_{total} ($=U_{tensile}+U_{shear}$), ▲: U^*_{total} (experimentally obtained).

γ_i and the measured modal fracture surface area S_i (type A specimen, $a/w=0.5$), and compare it with the measured total dissipation energy U^*_{total}. In Fig. 9, open circles denote $U_{tensile}$ ($=2\gamma_{tensile}S_{tensile}$), open squares denote U_{shear}($=2\gamma_{shear}S_{shear}$), open triangles denote U_{total}($=U_{tensile}+U_{shear}$), and closed triangles denote U^*_{total} which were experimentally obtained from the load/displacement curves. A good agreement between U_{total} and U^*_{total} can be seen in Fig. 9, indicating that the modal separation was performed successfully. As well, U_{total} is mostly occupied by $U_{tensile}$ independent of the heat treatment temperature, thus we can understand that the energy dissipation of these C/C composites is mainly characterized as the tensile fracture process with some contribution of the interlaminar shear fracture process. Each contribution of the fracture mode may be changed depending on matrix texture, fiber architecture, and heat treatment, etc. in other C/C composites. Therefore, this type of examination will be important for our understanding of the multi-modal fracture behavior of C/C composites and for maximizing their performance in structural applications at high temperatures.

5. Conclusions

Modal separation of work-of-fracture is performed on some C/C composites in order to characterize their multi-modal fracture behavior, and the modal work-of-fracture values for tensile and interlaminar shear modes are estimated as functions of the heat treatment temperature. The following conclusions are obtained in this study:

1. Modal separation of work-of-fracture is proposed based on the energy conservation law during fracture. The fundamental equation for the modal separation can be expressed as a linear combination of the modal work-of-fracture γ_i with a weighting function of the modal fracture surface area S_i.

2. Some C/C composites were prepared by heat treatment at temperatures between 1000°C and 2800°C. During work-of-fracture tests, tensile fracture and interlaminar shear fracture were simultaneously observed in these specimens. By plotting $U_{total}/2S_{total}$ against $S_{tensile}/S_{total}$, a close linear relationship is obtained in

each C/C composite, implying that the modal separation has been completed satisfactorily. By using linear regression analysis of the plots, the modal work-of-fracture values ($\gamma_{tensile}$ and γ_{shear}) are estimated within an acceptable level of accuracy. The $\gamma_{tensile}$ shows a maximum at a heat treatment temperature of 2000°C, whereas the γ_{shear} does not largely change with increasing the heat treatment temperature. Thus, the modal work-of-fracture constitutes a promising parameter for describing the multi-modal fracture of composite materials.

3. The $\gamma_{tensile}$ is verified using the fiber pullout energy, and interpreted with the sliding force at the fiber/matrix interface and the fiber pullout length. The γ_{shear} is suggested to correlate with the debris density on interlaminar shear fracture surfaces. This study quantitatively shows the contribution of each fracture mode to the total energy dissipation of the composites.

Acknowledgments

The authors wish to express their gratitude to Mr. M. Kano at Smitomo Metal Industries, Ltd. for his help in sample preparation and his helpful discussion. This research was partly supported by a Grant-in-Aid for Scientific Research (No. 09750760) from the Ministry of Education, Science and Culture of Japan, and a Grant-in-Aid for JSPS Fellows (No. 4458), and the Ishikawa Foundation for Carbon, Science and Technology.

References

1. E. FIZTER and L. M. MANOCHA, in "Carbon Reinforcements and Carbon/Carbon Composites" (Springer-Verlag, Berlin, 1998) p. 97.
2. T. R. GUESS and W. R. HOOVER, *J. Composite Materials* **7** (1973) 2.
3. L. R. HETTCHE and T. R. TUCKER, in "ASTM STP601" (American Society for Testing and Materials, 1976) p. 106.
4. J. X. ZHAO, R. C. BRADT and P. L. WALKER, in "Fracture Mechanics of Ceramics, vol. 6," edited by R. C. Bradt *et al*. (Plenum Press, New York, 1983) p. 107.
5. H. C. KIM, K. J. YOON, R. PICKERING and P. J. SHERWOOD, *J. Mater. Sci.* **20** (1985) 3967.
6. M. JENKINS, J. MIKAMI, T. CHANG and A. OKURA, *SAMPE J* **5/6** (1988) 32.
7. S. SENET, R. E. GRIMES, D. L. HUNN and K. W. WHITE, *Carbon* **29** (1991) 1039.
8. M. SAKAI, T. MIYAJIMA and M. INAGAKI, *Composites Science and Technology* **40** (1991) 231.
9. G. E. GRIESHEIM, P. B. POLLOCK and S. C. YEN, *J. Amer. Ceram. Soc.* **76** (1993) 944.
10. Y. M. MAI and K. M. PILKO, *J. Mater. Sci.* **14** (1979) 386.
11. K. YASUDA, S. TANAKA and Y. MATSUO, *ibid.* **34** (1999) 2331.
12. M. INAGAKI, in "Tanso-Zairyo-Nyumon" (The Carbon Society of Japan, 1972) p. 184 (in Japanese).
13. T. MIYAJIMA and M. SAKAI, in "Fracture Mechanics of Ceramics, vol. 9," edited by R. C. Bradt *et al*. (Plenum Press, New York, 1992) p. 83.

Received 14 August 2001
and accepted 21 February 2002